Spatial distribution of impact craters on Deimos

Hirata, Naoyuki

Title

Spatial distribution of impact craters on Deimos

Author

Naoyuki Hirata

Authors' affiliations

[a] Graduate School of Science, Kobe University, Kobe, Japan.

* Corresponding Author E-mail address: hirata@tiger.kobe-u.ac.jp

Proposed Running Head: Crater distribution on Deimos

Editorial Correspondence to:

Dr. Naoyuki Hirata

Kobe University

Rokkodai 1-1 657-0013

Tel/Fax +81-7-8803-6566

Email: hirata@tiger.kobe-u.ac.jp

Key Words

Mars, satellites

Impact processes

Geological processes

Cratering

Phobos and Deimos

Highlights

- This work studied the Deimos surface imaged at 43 m/pixel minimum resolution.
- Craters (D > 30 m) on the studied areas of Deimos are randomly distributed
- The size-frequency distribution slope is shallower in craters than in impactors
- Both of these observations are explained by seismic-shaking and ejecta emplacement

Abstract

Deimos, one of the Martian moons, has numerous impact craters. However, it is unclear whether crater saturation has been reached on this satellite. To address this issue, we apply a statistical test known as nearest-neighbor analysis to analyze the crater distribution of Deimos. When a planetary surface such as the Moon is saturated with impact craters, the spatial distribution of craters is generally changed from random to more ordered. We measured impact craters on Deimos from Viking and HiRISE images and found (1) that the power law of the size-frequency distribution of the craters is approximately −1.7, which is significantly shallower than those of potential impactors, and (2) that the spatial distribution of craters over 30 m in diameter cannot be statistically distinguished from completely random distribution, which indicates that the surface of Deimos is inconsistent with a surface saturated with impact craters. Although a crater size-frequency distribution curve with a slope of −2 is generally interpreted as indicating saturation equilibrium, it is here proposed that two competing mechanisms, seismic shaking and ejecta emplacement, have played a major role in erasing craters on Deimos and are therefore responsible for the shallow slope of this curve. The observed crater density may have reached steady state owing to the obliterations induced by the two competing mechanisms. Such an occurrence indicates that the surface is saturated with impact craters despite the random distribution of craters on Deimos. Therefore, this work proposes that the age determined by the current craters on Deimos reflects neither the age of Deimos itself nor that of the formation of the large

concavity centered at its south pole because craters should be removed by later impacts. However, a few of the largest craters on Deimos may be indicative of the age of the south pole event.

1. Introduction

Deimos, one of the two moons of Mars, has a mean diameter of 12 km. Relative to Phobos, the other Martian moon, Deimos is smaller, and its orbit is more distant from Mars. Many explorations to both moons have been conducted since the 1970s.

The Mariner 9 spacecraft was the first to capture images of Phobos and Deimos at a sufficient resolution for resolving surface features; these images reveal irregular shapes with numerous impact craters (Pollack et al. 1973, Pollack et al. 1972). The Viking Orbiters obtained higher-resolution images revealing many differences between the surfaces of the two moons; for example, (1) Phobos exhibits numerous linear depressions known as grooves that have not been identified on Deimos, (2) the surface of Deimos appears to be significantly smoother than that of Phobos, and (3) landforms on Deimos, which are rare on Phobos, are indicative of downslope movement of debris (Veverka and Duxbury 1977, Duxbury and Veverka 1977, Thomas 1979).

Notably, Deimos appears to have loose surface material that moves downslope from prominent ridges and accumulates in topographic lows as well as impact craters that are degraded and infilled via migration of regolith (Thomas and Veverka 1980b). Furthermore, Thomas et al. (1996) suggested that a 10-km concavity centered on the south pole was formed by a considerable impact (Thomas 1989), that generated ejecta blankets ~200 m thick across the surface of Deimos and created the notable differences in surface appearance between Deimos and Phobos.

The crater densities and crater size-frequency distributions (CSFD) of the two satellites are similar. Pollack et al. (1972) and Thomas and Veverka (1977) examined Mariner 9 images and found that the crater density on the surface of Phobos is close to saturation. However, a meaningful crater density curve could not be constructed for Deimos owing to the paucity of visible craters. Later, Thomas and Veverka (1980a) examined Viking images and reported (1) that the crater density at 1 km in diameter (D) on Deimos is almost the same as (0.7 times denser than) that on Phobos, and (2) that the slope of the cumulative CSFD curve for each satellite is approximately −1.9. Because crater saturation makes an apparent population follow an equilibrium line with a slope of −2 (Gault 1970), these slope curves indicate saturation equilibrium. As such, age determination by crater counting may not be useful in the case of Deimos.

The main purpose of this study is to investigate the crater saturation of Deimos. Evaluating the randomness of the spatial distribution of impact craters is suitable to detect this saturation. According to Squyres et al. (1997), the spatial distribution of observed craters transitions from random to more ordered because craters that form in sparse areas obliterate the relatively few existing craters and thereby fill in the sparseness, whereas craters that form in areas of existing crater clustering obliterate the existing craters and reduce the clustering. In fact, Squyres et al. (1997) demonstrated that the crater distributions of the heavily cratered terrains of Callisto and Rhea are ordered rather than random. This method has been applied to evaluate the distributions of craters on various solar system objects. For example, Phillips

et al. (1992) determined that the crater distribution on Venus has good agreement with a completely random distribution; therefore, the variation in crater density can be explained by the randomness of the crater production on that planet. Michael et al. (2012) analyzed two sites on Mars that are partially covered by lava flows and reported that a statistical test using the mean 2nd-closest neighbor distance can be a more sensitive measure of clustering than those using the mean closest neighbor distance. Schmedemann et al. (2014) adopted this methodology to determine whether the observed population is consistent with being accumulated on a homogeneous geological unit.

A further purpose of this work is to update the resources used for crater study by using images captured by the HiRISE camera onboard the Mars Reconnaissance Orbiter (MRO). The best resource previously available for studying craters on Deimos has been data from the Viking mission; incorporation of HiRISE images enables improved crater counting for the near side of Deimos.

2. Data and Methods

For crater counting, the following resources were utilized: (i) 25 images captured by the Viking orbiters, (ii) two images captured by the HiRISE camera, (iii) a shape model of Deimos developed by Thomas (1993), and (iv) two cylindrical projection maps of Deimos developed by Stooke (2012). All of these resources are available via the NASA Planetary Data System. Unfortunately, the images of Deimos obtained by the HRSC camera

onboard Mars Express are not as clear as those from the Viking mission. Consequently, these images were not used.

All impact craters were identified from the Viking and HiRISE images rather than from maps. The Viking images commonly include reseau marks, salt-and-pepper noise, and gaps; therefore it must be confirmed that a possible crater is not an artifact of such noise. Because most of the craters are largely degraded and infilled with regolith, and therefore often lack sharp shapes, bright circular albedo features and/or circular depressions were regarded as impact craters for this work.

The image resolution of the Viking and HiRISE images is far from uniform. To obtain unbiased crater density and distribution data, three study areas have been defined as Areas 1 (high), 2 (medium), and 3 (low). Figure 1 delineates the coverage of each area. In 1977, Viking 2 approached Deimos at a distance of several tens of kilometers and captured four high-resolution images as high as ~1 m/pixel: images 423B61, 423B62 (Fig. 2a), 423B63, and 423B64. Because the coverage of image 423B64 is quite limited, it was omitted from this analysis. The region covered by the three remaining high-resolution images is defined as Area 1, which covers a small fraction of the surface near the north pole. This region has an area of 6.2 km^2, or 1.2% of the total surface area of Deimos. To ensure that the evaluation of crater counting was not affected by image resolution, D = 20 m was set as the minimum diameter threshold in Area 1. The area covered at medium resolution, between 14 and 20 m/pixel, is defined as Area 2. This region is represented by four Viking images (428B59, 428B60, 428B61, and 428B62)

and two HiRISE images (ESP_012068_9000 and ESP_012065_9000) (Fig. 2b). This region has an area of 175.0 km^2, or 33.5% of the total surface area. The minimum diameter threshold in Area 2 was set at D = 200 m. Area 3, defined by low-resolution images of Deimos with resolutions higher than 43 m/pixel (Fig. 2c), is covered by 18 Viking images (413B83–86, 433B31–42, 433B55–56) and the six images used for Area 2. This region has an area of 262.9 km^2, or 50.4% of the total surface area of Deimos. The minimum diameter threshold in Area 3 was set at D = 400 m. Although the trailing hemisphere was imaged at 31 m/pixel (Fig. 2d), this area was not included in this study. It should be noted that Area 1 falls within Area 2, which in turn falls within Area 3, and the area they cover is primarily on the leading hemisphere of Deimos. The ISIS 3 software produced by the United States Geological Survey was used to calibrate the raw images.

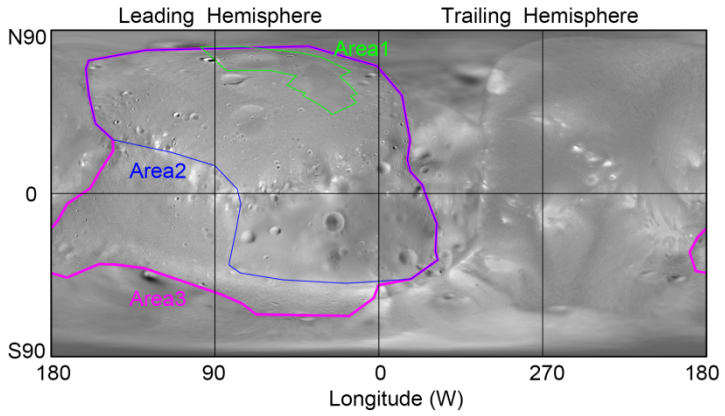

Figure 1 Global map of Deimos in simple cylindrical projection. The three study areas (Areas 1, 2, and 3) are outlined on the map.

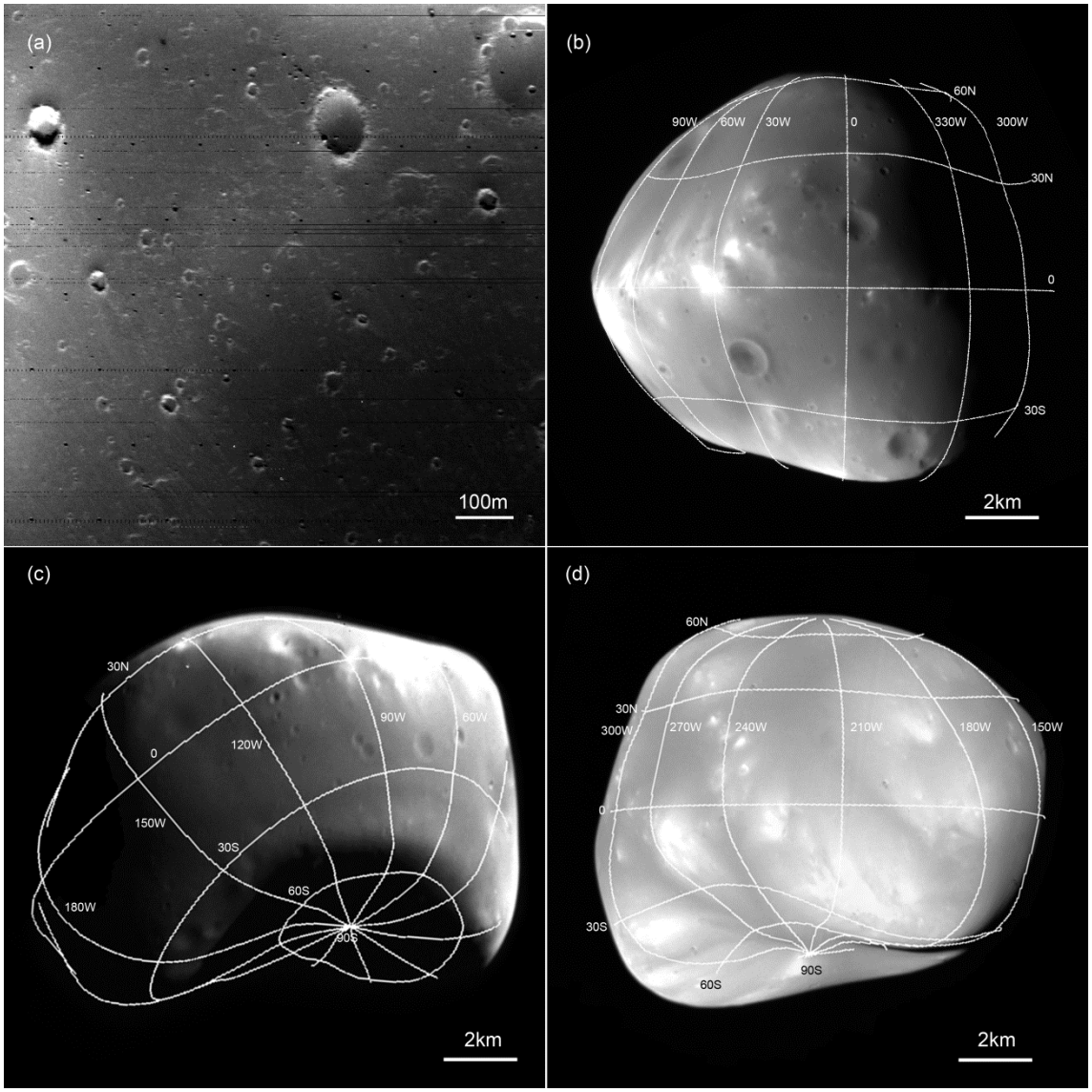

Figure 2 (a) One of the highest resolution images of Deimos (423B62), which shows a part of Area 1. The center is located at 30°W and 57°N. (b) A HiRISE image of Deimos, with a resolution of 20 m/pixel (ESP_012068_9000). (c) Example of a Viking image that shows Area 3 (433B56). This image shows most of the leading hemisphere of Deimos at a resolution of 34 m/pixel. (d) Trailing hemisphere of Deimos at a resolution of 31 m/pixel (507A01).

The Small Body Mapping Tool (Kahn et al. 2011) was used to measure the diameters and locations of craters for this study. This software enabled identification and measurement of the centers and diameters of craters based on three points selected along the crater rim on maps prepared by Stooke (2012) rendered onto a shape model by Thomas (1993) (Fig. 3). The shape model is defined by a 5° grid of longitude and latitude. Stooke's maps include a global map and a high-resolution local map. The global map has a resolution of 0.05°/pixel and is used for counting craters in Areas 2 and 3, whereas the local map has a resolution of 0.025°/pixel and is used for counting craters in Area 1.

To compare the counting results for Deimos and Phobos, the Phobos crater database developed by Salamunićcar et al. (2014) was utilized, which includes a complete dataset of craters of $D > 50$ m across all of Phobos from images captured by the HRSC onboard the Mars Express. To determine crater densities, the surface area of Phobos was assumed to be 1588 km^2, on the basis of an ellipsoid shape with semi-axis lengths of 13.03 km × 11.40 km × 9.14 km.

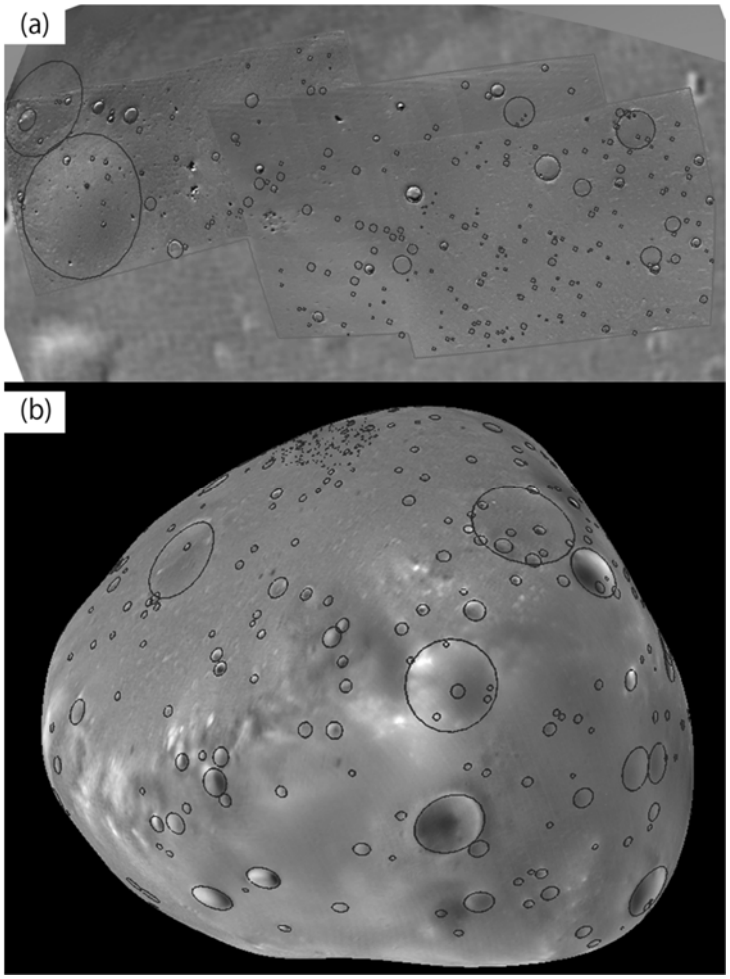

Figure 3 Examples of the identification of impact craters; (a) high resolution, Area 1; (b) medium resolution, Area 2.

3. Analysis

To analyze the randomness of the spatial distribution of craters, this study followed the methodology of Squyres et al. (1997) to perform a statistical test known as nearest-neighbor analysis. The distances between each point and its nearest neighboring point were determined and averaged, and the observed mean distance was compared with the mean distance

231 expected under random distribution. If the observed value was significantly
232 smaller (greater) than the expected value, the distribution was considered to
233 be clustered (ordered).

234 If we assume a Poisson process, the expected mean distance between
235 each point and its nearest neighboring point is given by

236 $$d_{exp} = \frac{1}{2\sqrt{n/A}} \text{ , (1)}$$

237 where n is the number of craters and A is the area of the study region (Clark
238 and Evans 1954). The standard deviation (σ) of this value is obtained by

239 $$\sigma = \sqrt{\frac{(4-\pi)A}{4\pi n^2}} \text{ . (2)}$$

240 Following Squyres et al. (1997), the Z-statistic was also determined to assess
241 the degree by which the value of the observed mean distance (d_{obs}) deviates
242 from randomness:

243 $$Z \equiv \frac{d_{obs}-d_{exp}}{\sigma} \text{ . (3)}$$

244 The observed distance between two points was determined on the basis of
245 the length of the line segment between the two points in a Cartesian
246 coordinate system centered at the geometric center of Deimos. This was
247 considered because the shape of Deimos is far from ellipsoid or spherical, and
248 measurement using projected coordinates is not appropriate. A positive
249 (negative) Z value indicates that the distribution of points is considered to be
250 more ordered (clustered), whereas a value of Z close to 0 indicates that the
251 distribution cannot be distinguished from random. The value of Z was
252 obtained for the distribution of all craters that exceeded a given diameter.

253 The Z-statistic was not calculated if the number of craters was lower than 15,
254 although a value can be calculated provided that n > 2. This limitation was
255 applied because the line segments between craters deviate from the surface
256 of Deimos when the number of craters was below 15.

257 It should be noted that Eq. (1) is valid when distances to obtain
258 nearest neighbors are allowed to cross the boundary of the study area (Clark
259 and Evans 1954). When the area under study is limited, the boundary effects
260 are expected to influence the value of d_{exp} and σ and thus to bias the
261 measurements of Z. Thus, this work numerically computed the value of d_{exp}
262 and σ using the Monte Carlo simulation (MC) in combination with the
263 actual boundary. Specifically, this work considered that (1) points with a
264 number of n were produced on the actual surfaces of the study areas of
265 Deimos or Phobos, (2) these points were generated by uniformly distributed
266 random numbers on a sphere because impactors are assumed to originate
267 from all directions of the satellites, (3) the mean nearest neighboring distant
268 (d_i in i^{th} trial) was measured by the average of the lengths defined by the line
269 segment between the two points, (4) based upon these three assumption,
270 10000 trials were performed, and (5) the average and deviation of d_i (i = 1,2,3,
271 …10000) were obtained as d_{exp} and σ, respectively. As a result, d_{exp} and σ
272 are shown in Tables 1 and 2. It should be note that n is from Table 3 in the
273 Results section, and d_{exp} and σ in Table 1 and 2 correspond to each bin in
274 Table 3.

275

276 **Table 1.** Expected mean distance (d_{exp} in km) for each bin derived from Eq. (1)

277 and Monte Carlo simulation (MC). The value of *n* corresponds to that in
278 Table 3.

	Phobos		Deimos Area 1		Deimos Area 2		Deimos Area 3	
	Eq. 1	MC	Eq.1	MC	Eq.1	MC	Eq. 1	MC
D > 20m	-	-	0.098425	0.107629	-	-	-	-
D > 30m	-	-	0.135840	0.150720	-	-	-	-
D > 40m	-	-	0.172649	0.194396	-	-	-	-
D > 50m	0.247423	0.245575	0.227303	0.261454	-	-	-	-
D > 60m	0.273792	0.271738	0.293447	0.349813	-	-	-	-
D > 70m	0.306973	0.304766	0.301954	0.359033	-	-	-	-
D > 80m	0.330660	0.328273	0.311247	0.372274	-	-	-	-
D > 90m	0.356313	0.353662	-	-	-	-	-	-
D > 100m	0.388081	0.385168	-	-	-	-	-	-
D > 150m	0.534042	0.529847	-	-	-	-	-	-
D > 200m	0.647813	0.643680	-	-	0.713247	0.725484	-	-
D > 300m	0.882288	0.873824	-	-	1.059148	1.105333	-	-
D > 400m	1.160070	1.153331	-	-	1.479020	1.574016	1.654854	1.747210
D > 500m	1.449320	1.438911	-	-	1.604222	1.730160	1.910861	2.032343
D > 600m	1.734236	1.720674	-	-	-	-	2.026774	2.162458
D > 700m	1.899761	1.892214	-	-	-	-	-	-
D > 800m	2.241722	2.227525	-	-	-	-	-	-
D > 900m	2.398671	2.381145	-	-	-	-	-	-
D > 1km	2.662571	2.642330	-	-	-	-	-	-
D > 1.5km	3.637765	3.584959	-	-	-	-	-	-
D > 2km	4.154620	4.130836	-	-	-	-	-	-
D > 3km	4.981215	4.986887	-	-	-	-	-	-

279

280

281 **Table 2.** Standard deviation (σ in km) of d_{exp} for each bin derived from Eq. (2)
282 and Monte Carlo simulation (MC). The value of *n* corresponds to that in
283 Table 3.

	Phobos	Deimos Area 1	Deimos Area 2	Deimos Area 3

	Eq.2	MC	Eq.2	MC	Eq.2	MC	Eq.2	MC
D > 20m	-	-	0.004067	0.004644	-	-	-	-
D > 30m	-	-	0.007747	0.009148	-	-	-	-
D > 40m	-	-	0.012515	0.015403	-	-	-	-
D > 50m	0.001606	0.001623	0.021693	0.027543	-	-	-	-
D > 60m	0.001967	0.001991	0.036155	0.048396	-	-	-	-
D > 70m	0.002472	0.002502	0.038281	0.051330	-	-	-	-
D > 80m	0.002868	0.002893	0.040674	0.055764	-	-	-	-
D > 90m	0.003331	0.003337	-	-	-	-	-	-
D > 100m	0.003951	0.003945	-	-	-	-	-	-
D > 150m	0.007482	0.007505	-	-	-	-	-	-
D > 200m	0.011010	0.010588	-	-	0.040203	0.043424	-	-
D > 300m	0.020422	0.019430	-	-	0.088654	0.101022	-	-
D > 400m	0.035306	0.034034	-	-	0.172874	0.203131	0.176574	0.197038
D > 500m	0.055107	0.053106	-	-	0.203382	0.239876	0.235432	0.270798
D > 600m	0.078903	0.078185	-	-	-	-	0.264860	0.310710
D > 700m	0.094684	0.093189	-	-	-	-	-	-
D > 800m	0.131838	0.140942	-	-	-	-	-	-
D > 900m	0.150945	0.156222	-	-	-	-	-	-
D > 1km	0.185985	0.185331	-	-	-	-	-	-
D > 1.5km	0.347173	0.306003	-	-	-	-	-	-
D > 2km	0.452834	0.442926	-	-	-	-	-	-
D > 3km	0.650949	0.601729	-	-	-	-	-	-

4. Results

On the surface of Deimos, 510 craters were identified: 236 craters in Area 1, 215 craters in Area 2 outside of Area 1, 38 craters in Area 3 outside of Area 2, and 21 craters on the remaining regions of Deimos (Fig. 4). The diameters and locations of the identified craters are listed in Supplementary Table S1. Figure 5a shows the cumulative CSFDs of Deimos and Phobos. This analysis followed the method of the Crater Analysis Technique Working

293 Group (1979).

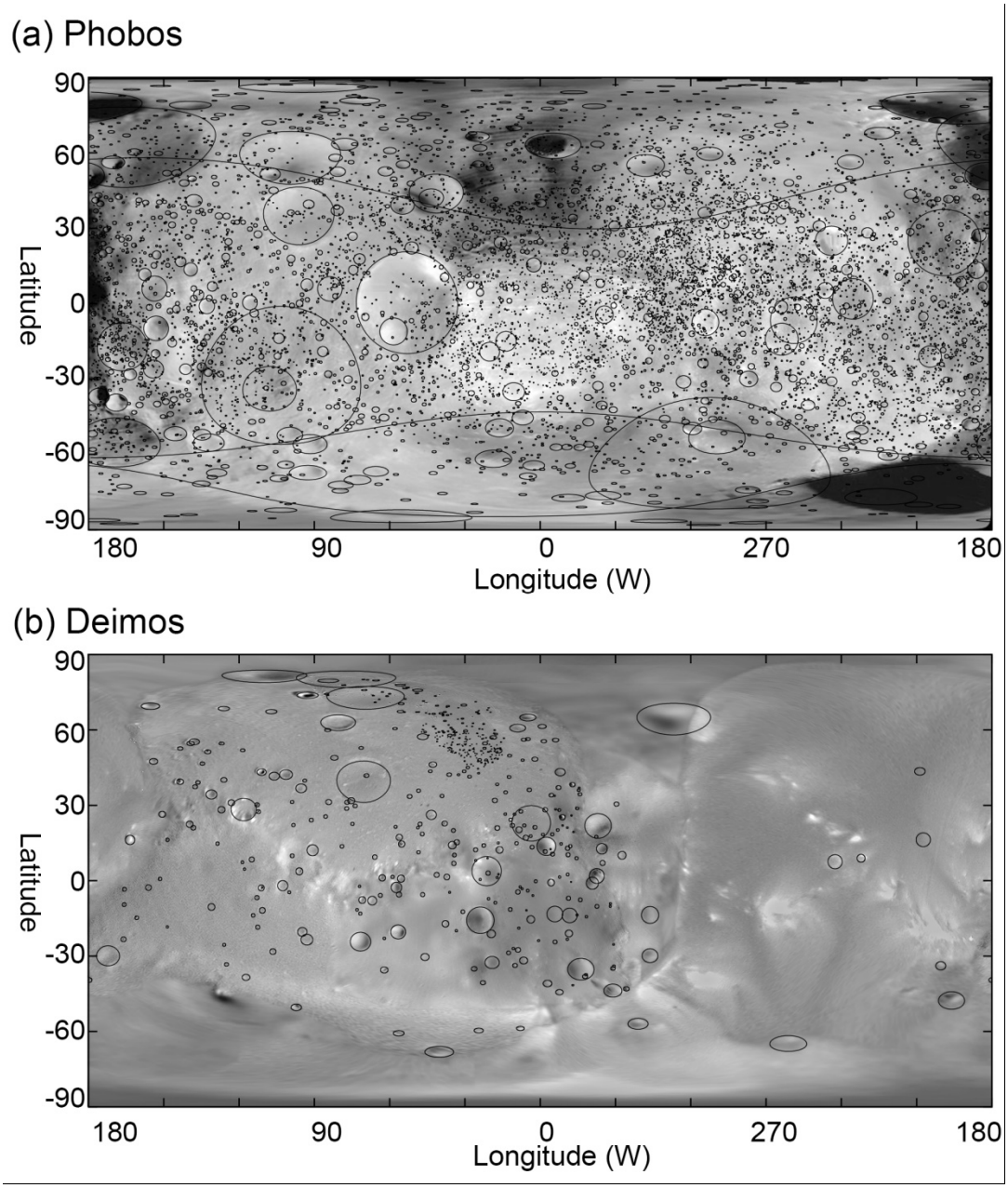

294

295 **Figure 4** (a) Global distribution of craters on Phobos derived from
296 Salamunićcar et al. (2014). The lines outline crater rims. (b) Global
297 distribution of craters identified on Deimos. Both maps are shown in simple
298 cylindrical projection. The global mosaics for Phobos and Deimos are from
299 Willner (2008) and Stooke (2012), respectively.

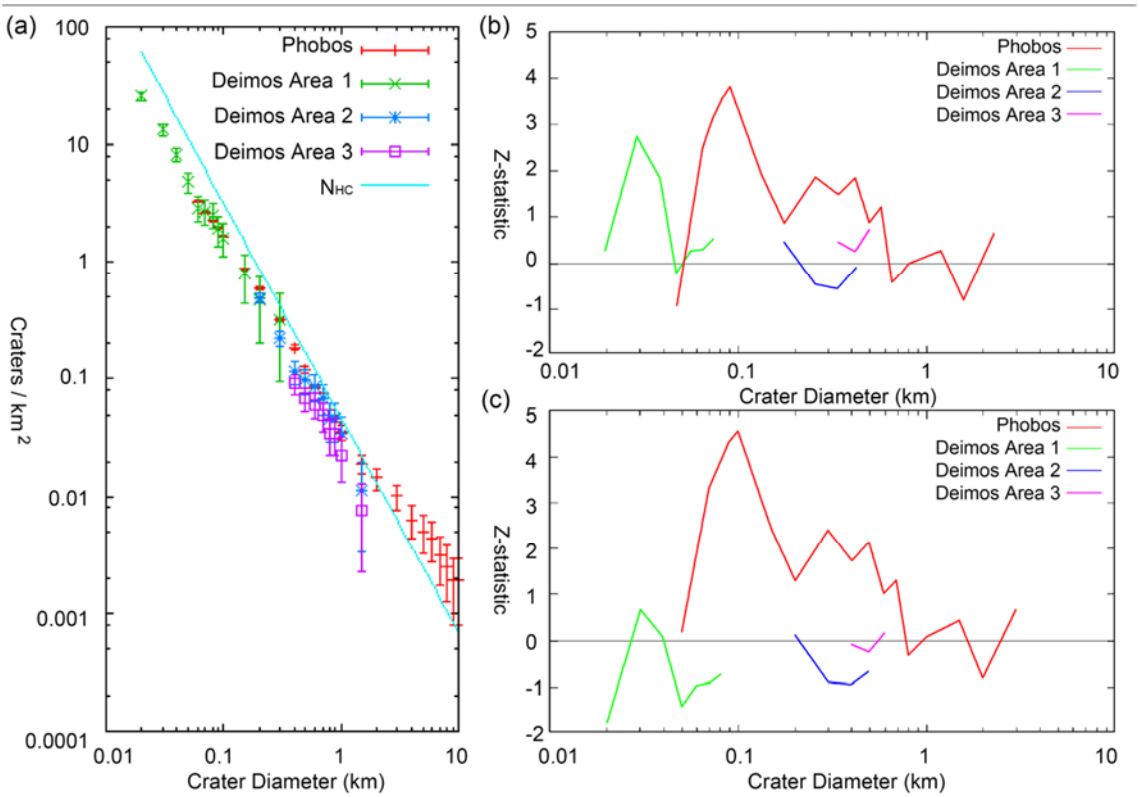

Figure 5 (a) Cumulative CSFD of impact craters on Phobos and the three study areas of Deimos. The line is from Eq. (4). (b) Values of Z-statistics in d_{exp} and σ defined by Eq. (1) and (2). The values of Z in each bin, shown in Table 3, are defined by all craters larger than a given diameter. (c) Values of Z-statistics in d_{exp} and σ obtained by Monte Carlo simulation.

Table 3. Numbers of observed craters and observed mean distance (d_{obs} in km) for each bin.

	Phobos		Deimos Area 1		Deimos Area 2		Deimos Area 3	
	n	d_{obs}	n	d_{obs}	n	d_{obs}	n	d_{obs}
D > 20m	-	-	160	0.0994	-	-	-	-
D > 30m	-	-	84	0.1569	-	-	-	-
D > 40m	-	-	52	0.1958	-	-	-	-

D > 50m	6485	0.2459	30	0.2220	-	-	-	-
D > 60m	5296	0.2752	18	0.3027	-	-	-	-
D > 70m	4213	0.3131	17	0.3121	-	-	-	-
D > 80m	3631	0.3396	16	0.3318	-	-	-	-
D > 90m	3127	0.3681	12	-	-	-	-	-
D > 100m	2636	0.4031	10	-	-	-	-	-
D > 150m	1392	0.5483	5	-	-	-	-	-
D > 200m	946	0.6570	3	-	86	0.7303	-	-
D > 300m	510	0.9200	2	-	39	1.0131	-	-
D > 400m	295	1.2112	2	-	20	1.3776	24	1.7265
D > 500m	189	1.5508	2	-	17	1.5735	18	1.9647
D > 600m	132	1.7994	2	-	15	-	16	2.2125
D > 700m	110	2.0133	1	-	12	-	13	-
D > 800m	79	2.1809	1	-	12	-	9	-
D > 900m	69	2.3595	1	-	8	-	9	-
D > 1km	56	2.6545	0	-	6	-	6	-
D > 1.5km	30	3.7169	0	-	2	-	2	-
D > 2km	23	3.7685	0	-	0	-	0	-
D > 3km	16	5.3799	0	-	0	-	0	-

No significant difference in crater density was detected between Phobos and Deimos. The crater densities at D = 100 m for Phobos were 0.89, 0.94, and 1.03 times higher than those of Deimos in Areas 1, 2, and 3, respectively. This finding is in good agreement with the previous report by Thomas and Veverka (1980a). On Deimos, the power law of CSFD is −1.66 ± 0.05 for Area 1, −1.70 ± 0.10 for Area 2, and −1.81 ± 0.20 for Area 3; that on Phobos is −1.49. These values are slightly shallower than the value of −1.9 obtained by Thomas and Veverka (1980a).

The crater density for Phobos and Deimos is roughly half of the

heavily cratered lunar surface. According to Hartmann (1984) and Trask (1966), the crater density on a planetary surface saturated with craters approaches a single level of crater density because of the steady state. The level follows the relation

$$\log N_{HC} = -1.83 \log D - 1.33 \quad , (4)$$

where N_{HC} is the crater density of heavily cratered surfaces such as the lunar surface and D is the crater diameter in kilometers. Compared with Eq. (4), the crater densities at D = 100 m for Phobos and Area 1 of Deimos are 0.46 times and 0.52 times that of N_{HC}, respectively.

Figures 5b and 5c show the Z-statistics for craters on Phobos and Deimos from Eqs. (1)/(2) and Monte Carlo simulation, respectively. Based on Fig. 5b, the Z-statistics of craters in Areas 2 and 3 and those of craters with D > 50 m in Area 1, are close to 0. Although craters with D < 40 m in Area 1 have a Z-statistic larger than +2 in Fig. 5b, this may be invalid because Fig. 5c shows a Z-statistic close to 0. These findings indicate that the distribution of craters larger than 30 m cannot be distinguished from random distribution. This indicates that the surface of Deimos is inconsistent with heavily cratered surfaces such as the Moon, Callisto, or Rhea. For comparison, the Z-statistic of craters on Phobos with D > 150 m is smaller than +2, whereas it is larger than +2 for D < 100 m, although the Z-statistic of craters on Phobos with D < 500 m is close to +2. The Z-statistics for craters with the smallest diameters recorded on Deimos (D = 20 m) and on Phobos (D = 50m) differ significantly from other bins, which can be attributed to bias in the crater identification.

345

346 ## 5. Discussion

347 The observed slope of the CSFD curve for Deimos, at approximately
348 −1.7, is much shallower than that of potential impactors. In particular, on
349 the Moon and Mars, the crater production functions follow a slope of −3.8 for
350 craters of D < 1.41 km (Ivanov et al. 2002), and in most cases the CSFD
351 slopes generated by secondary impactors are significantly steeper than −3.
352 In short, Deimos lacks small craters. Although its shallow CSFD implies
353 saturation with craters, the randomness of the distribution contradicts this
354 theory.

355 In contrast, the shallow CSFD slope of Deimos is fairly consistent
356 with those observed on Eros and Itokawa. It has been reported that
357 impact-induced seismic shaking on these small asteroids preferentially
358 erases smaller craters and generates a shallower CSFD (e.g., Hirata et al.
359 2009, Richardson et al. 2004). Ejecta emplacement is also a possible cause of
360 crater erasure; ejecta generated by numerous impactors could have
361 resurfaced large areas of Deimos (Nayak et al. 2016, Thomas 1998). To
362 evaluate the efficiency of these two alternative mechanisms, a case study for
363 impactors with diameters of D_i = 0.1 m, 1 m, and 10 m was performed. These
364 impactors formed transient craters on Deimos with diameters of 39 m, 233 m,
365 and 1402 m, respectively (Appendix A).

366 ### 5.1. Seismic shaking on Deimos

367 First, impact-induced seismic shaking on Deimos was evaluated.
368 According to Miyamoto et al. (2007) and Richardson et al. (2005), the ratio of

the maximum impact-induced seismic acceleration, a, and the gravity of Deimos, g (= 0.003 m/s^2; Murchie et al. 2015), is given by

$$\frac{a}{g} \sim \frac{3 f v_i}{G} \sqrt{\eta \frac{\rho_i}{\rho_d^3} \frac{D_i^3}{D_d^5}} \quad , (5)$$

where f is the seismic frequency (1–100 Hz), v_i is the impactor velocity, G is the gravitational constant (6.673×10^{-11} m^{3}kg^{-1}s^{-2}), η is the seismic efficiency factor (~10^{-4}), ρ_i is the density of the impactor (assumed as 2500 kg m^{-3}), ρ_d is the density of Deimos (1490 kg m^{-3}; Murchie et al. 2015), D_i is the impactor diameter (0.1 m, 1 m, or 10 m), and D_d is the diameter of Deimos (12 km; Thomas 1993). Following Schmedemann et al. (2014), the impactor velocity on Deimos (v_i) averages 8.2 km/s, based on

$$v_i = \sqrt{v_{impM}^2 - v_{escM}^2 + v_{escD}^2}, \quad (6)$$

where v_{impM} is the mean impactor velocity on Mars (9.4 km/s), v_{escM} is the escape velocity at the Martian surface (5 km/s), and v_{escD} is the escape velocity of Mars at the orbit of Deimos (1.9 km/s). As a result, we can obtain a/g = 0.006–0.6 for D_i = 0.1 m, a/g = 0.2–20 for D_i = 1 m, and a/g = 6–600 for D_i = 10 m (Fig. 6a). Large impactors (D > 0.1 m) can induce seismic acceleration exceeding the surface gravity, which is expected to be sufficient for moving particles over the surface. In contrast, small impactors (D < 0.1 m) would locally rather than globally induce such movement.

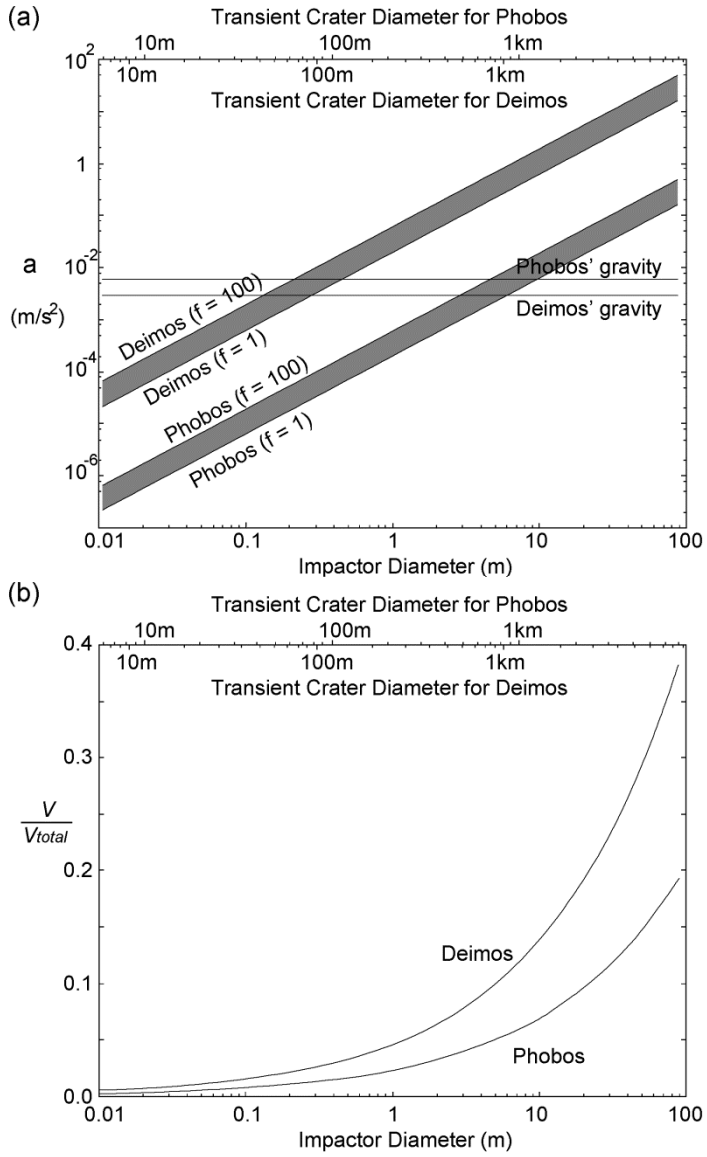

Figure 6. (a) Maximum seismic acceleration induced by impactors, based on Eq. (5). Gray regions indicate the values from Eq. (5) for a range of seismic frequency (f = 1–100 Hz). The transient crater diameter (upper horizontal axis) that corresponds to an impactor diameter (lower horizontal axis) is calculated as that defined in Appendix A. (b) The ratio of the volume that moved faster than 5 m/s to the total volume of ejecta, based on Eq. (9) when v_{ej} = 5 m/s.

396

397 ### 5.2. Ejecta emplacement on Deimos

398 An additional mechanism of ejecta emplacement on Deimos was
399 considered. Following Nayak et al. (2016), the volume of ejected particles
400 that moved faster than a given velocity (v_{ej}) in the gravity regime is given by

401 $$V_{ejecta} = 0.3R^3 \left(\frac{v_{ej}}{\sqrt{gR}}\right)^{-1.2}, \quad (7)$$

402 where R is the crater radius (Housen and Holsapple 2011). We assumed R =
403 $0.5D_{tc}$, where D_{tc} is the transient crater diameter. It should be noted that
404 because the surface of Deimos is covered by a thick regolith layer made of
405 noncohesive material (Thomas et al. 1996), gravity (strength) regime
406 cratering is plausible (unlikely). Based on the Maxwell's Z model, the total
407 volume of ejecta (V_{total}) from a crater is given by

408 $$V_{total} = \frac{z-2}{z+1} V_{tc}, \quad (8)$$

409 where V_{tc} is the volume of the transient crater and z is a constant generally
410 equal to 3 (Melosh 2011). If it is assumed that V_{tc} is equal to the volume of a
411 hemisphere with a diameter of D_{tc}, the volume that moved faster than a
412 given velocity (v_{ej}) relative to the total volume of ejecta is given by

413 $$\frac{V}{V_{total}} = 0.38 \; v_{ej}^{-1.2} g^{0.6} D_{tc}^{0.6} \; . \quad (9)$$

414 The fate of ejecta roughly depends on v_{ej} as follows: (i) The ejecta
415 material launched at v_{ej} < 5 m/s (i.e. smaller than the escape velocity of
416 Deimos) will immediately reaccumulate on Deimos; (ii) material launched at
417 5 m/s < v_{ej} < 400 m/s will temporarily orbit Mars and eventually

418 reaccumulate on Deimos; (iii) material launched at 400 m/s < v_{ej} < 1900 m/s
419 will either hit Mars or its satellites or escape from the Mars system; and (iv)
420 material launched at v_{ej} > 1900 m/s will immediately escape from the Mars
421 system (Nayak et al. 2016). Based on Eq. (9), the volume able to escape from
422 Deimos (v_{ej} > 400 m/s) is negligible (< 0.1%); therefore, nearly all ejecta from
423 Deimos reaccumulate on Deimos.

424 Based on Eq. (8), the total volume of ejecta generated by an impactor
425 is 3.8×10^3 m^3 for an impactor of D_i = 0.1 m, 8.2×10^5 m^3 for D_i = 1 m, and 1.8
426 $\times 10^8$ m^3 for D_i = 10 m. If a total area of 521.6 km^2 for Deimos and uniform
427 distribution of ejecta over the surface are assumed, the depths of
428 reaccumulated ejecta from these impacts would be 7.2×10^{-6} m, 1.5×10^{-3} m,
429 and 0.34 m, respectively. Following these calculations and assuming that
430 final crater diameters are equal to the transient diameters, even the craters
431 identified in this study could generate ejecta emplacement with depths up to
432 3.9 m over the surface. Therefore, ejecta emplacement could contribute to
433 sufficient removal of smaller craters.

434 However, ejecta generated by a small impactor preferentially affect
435 the area nearest the impact site, whereas a large impactor will affect the
436 surface more globally because ejecta generated by larger impactors include
437 larger volumes of ejecta launched at 5 m/s < v_{ej} < 400 m/s. For example, from
438 Eq. (9), at v_{ej} = 5 m/s, the volume launched at v_{ej} > 5 m/s is 1.5% of the total
439 for D_i = 0.1 m, 4.4% for D_i = 1 m, and 13% for D_i = 10 m (Fig. 6b). Therefore,
440 almost all ejecta generated by small impactors (D_i < ~0.1 m) cannot escape
441 from Deimos and accumulate near the sites of impact. However, some of the

ejecta generated by large impactors (D_i > 10 m) will escape and reaccumulate widely across the surface of Deimos.

5.3. Crater erasure mechanisms and randomness of the crater distribution

Overall, the two mechanisms induced by large impactors (D_i > 0.1 m) appear to have affected and degraded most existing craters globally across the surface of Deimos, although small impactors (D_i < ~0.1 m) would preferentially erase existing craters near their sites of impact. This may be responsible for the random distribution of large craters (D > 30 m).

A new impact crater on Rhea or Callisto modifies existing craters in its surrounding area within a particular radius from its impact site. Its ejecta and evacuation prohibit adjacent craters from coinciding with each other spatially, which lengthens the average nearest-neighbor distance relative to random distribution. Consequently, the spatial distributions of craters on Rhea and Callisto have progressed from random to more ordered. However, a large impactor on Deimos modifies existing craters globally, rather than strictly near its impact site; therefore, random distribution of large craters is expected to be maintained.

This argument implies the possibilities that the surface of Deimos is heavily cratered and quite old and that the crater density currently observed on Deimos may reach the steady state crater density, even though the crater distribution is random. Such conditions imply the surface of Deimos is still saturated with impact craters. Perhaps the crater age reflects neither the

age of Deimos itself nor the excavation of its south pole, although the small number of largest craters on Deimos may indicate either case. Furthermore, the spatial distribution of craters on small bodies such as asteroids may not transition from random to more ordered, even if the surface is saturated with craters.

5.4. Comparison with Phobos

This concept may be applicable to Phobos as well. As shown in Figure 6, Eqs. (5) and (9) are applied for the case of Phobos, adopting its gravity (g = 0.006 m/s^2; Murchie et al. 2015), the escape velocity from its surface (v_{ej} = 11.4 m/s), its density ($\rho_d = \rho_t$ = 1860 kg m^{-3}; Murchie et al. 2015), its mean impactor velocity (v_i = 8.5 km/s; Schmedemann et al. 2014), and its diameter (D_d = 22.5 km; Thomas 1993). Based on Eqs. (5) and (A) in the Appendix, the value for a transient crater diameter of 39 m on Deimos is equivalent to that for a transient crater diameter of 74 m on Phobos. From Eqs. (9) and (A), the value for a transient crater diameter of 39 m on Deimos is equivalent to that of a transient crater diameter of 190 m on Phobos. These results have good agreement with the observed difference between randomly distributed large craters and orderly distributed small craters on Phobos. Therefore, as on Deimos, seismic shaking and ejecta emplacement play major roles in erasure of smaller crater on Phobos, and the shallow slope of the CSFD curve of Phobos may be explained by these two mechanisms. In this case, as for Deimos, age determination based on crater counting may be inapplicable for Phobos, even if its crater distribution is random.

Similarly, this work predicts that sufficiently smaller craters on

Deimos as well as Phobos are distributed orderly. Higher resolution images obtained by future exploration would allow research of smaller craters (D < 20m). The crater distribution and density of such craters may be determined by the obliteration of existing craters strictly near the impact site.

6. Conclusion

Impact craters on Deimos were recounted based on the basis of both Viking and HiRISE images covering the leading hemisphere of Deimos. No significant difference in crater density was noted between Phobos and Deimos; however, their crater density is roughly half that of the heavily cratered lunar surface. The power law of the cumulative CSFD for Deimos is approximately −1.7. A randomness analysis of the crater distribution on Deimos indicates that craters larger than D = 30 m are randomly distributed. A randomness analysis of the crater distribution on Phobos indicates that craters larger than D = 150 m are randomly distributed, whereas smaller craters are orderly distributed.

The shallow slope of the observed CSFD curve on Deimos can be plausibly explained by two mechanisms: impact-induced seismic shaking and/or ejecta emplacement. Theoretical models indicate that these two mechanisms, both induced by large impactors, can affect the area across the surface of the satellite. This may contribute to the maintenance of random distribution of large craters (D > 30 m).

In contrast, the effects of these two mechanisms may affect only the area in the immediate neighborhood of the impact sites when induced by

small impactors. This can explain the ordered distribution of small craters on Phobos (D < 100 m), which is similar to the ordered distribution of craters on Rhea and Callisto. These differences may be responsible for the difference observed between the random distribution of large craters (D > 150 m) and the ordered distribution of small craters on Phobos.

Therefore, Deimos may be a significantly cratered object (or may be saturated with craters) even though its crater distribution cannot be distinguished from random distribution. Thus, its crater age may be regarded as reflecting neither the age of Deimos itself nor the age of the large impact centered on its south pole.

Appendix A.

According to Melosh (2011), in gravity regime cratering, the transient crater diameter (D_{tc}) can be estimated by

$$D_{tc} = 1.161 \left(\frac{\rho_i}{\rho_t}\right)^{\frac{1}{3}} D_i^{0.78} v_i^{0.44} g^{-0.22} sin^{1/3}\theta \quad , \text{(A)}$$

where ρ_i is the density of the impactor (assumed as 2500 kg m^{-3}), ρ_t is the target density, D_i is the impactor diameter (0.1 m, 1m, or 10 m), v_i is the average impactor velocity, g is the gravity, and θ is the angle of impact from the horizontal (assumed as 45°). For Deimos, we used ρ_t = 1490 kg m^{-3}, v_i = 8.2 km/s, and g = 0.003 m/s^2. For Phobos, we used ρ_t = 1860 kg m^{-3}, v_i = 8.5 km/s, and g = 0.006 m/s^2.

Acknowledgements

The author wishes to thank Dr. Greg Michael and an anonymous reviewer for their comments, which significantly tightened the manuscript. In addition, the author would like to offer special thanks to Hiroshi Kikuchi at the University of Tokyo, who provided helpful comments for improving this work. This work is supported in part by Grant-in-Aid for JSPS Fellows. Images obtained by Viking orbiters and MRO are freely available via NASA's Planetary Data System (http://pds.nasa.gov). As well, the maps of Deimos are released in http://sbn.psi.edu/pds/asteroid/MULTI_SA_MULTI_6_STOOKEMAPS_V2_0/data/m2deimos/, and the shape model of Deimos is released in http://sbn.psi.edu/pds/asteroid/EAR_A_5_DDR_SHAPE_MODELS_V2_1/data/. Small Bodies Mapping Tool is released in http://sbmt.jhuapl.edu/index.html, and the ISIS3 software is released in https://isis.astrogeology.usgs.gov/.

References

Clark, P. J. & F. C. Evans (1954) Distance to Nearest Neighbor as a Measure of Spatial Relationships in Populations. *Ecology,* 35, 445-453.

Crater Analysis Techniques Working Group (1979). Standard Techniques for Presentation and Analysis of Crater Size-Frequency Data, Icarus, 37, 467-474.

Duxbury, T. C. & J. Veverka (1977) Viking imaging of Phobos and Deimos: An overview of the primary mission. *Journal of Geophysical Research,* 82, 4203-4211.

Gault, D. E. (1970) Saturation and Equilibrium Conditions for Impact Cratering on the Lunar Surface: Criteria and Implications. *Radio Science,* 5, 273-291.

Hartmann, W. K. (1984) Does Crater "Saturation Equilibrium" Occur in the Solar System? *Icarus*, 60, 56-74.

Hirata, N., O. S. Barnouin-Jha, C. Honda, R. Nakamura, H. Miyamoto, S. Sasaki, H.

565 Demura, A. M. Nakamura, T. Michikami, R. W. Gaskell & J. Saito (2009) A survey of
566 possible impact structures on 25143 Itokawa. *Icarus,* 200**,** 486-502.
567 Housen, K. R. & K. A. Holsapple (2011) Ejecta from impact craters. *Icarus,* 211**,** 856-875.
568 Ivanov, B., G. Neukum, W. Bottke & W. Hartmann. 2002. The comparison of size-frequency
569 distributions of impact craters and asteroids and the planetary cratering rate. In
570 *Asteroids III,* eds. W. F. B. Jr., A. Cellino, P. Paolicchi & R. P. Binzel, 89-101. Tucson:
571 The University of Arizona Press.
572 Kahn, E. G., O. S. Barnouin, D. L. Buczkowski, C. M. Ernst, N. Izenberg, S. Murchie & L. M.
573 Prockter. 2011. A Tool for the Visualization of Small Body Data. In *42nd Lunar and*
574 *Planetary Science Conference*, Abstract #1618. Houston: Lunar and Planetary
575 Institute.
576 Melosh, H. J. 2011. *Planetary surface processes*. Cambridge University Press.
577 Michael, G. G., T. Platz, T. Kneissl & N. Schmedemann (2012) Planetary surface dating from
578 crater size–frequency distribution measurements: Spatial randomness and
579 clustering. *Icarus,* 218**,** 169-177.
580 Miyamoto, H., H. Yano, D. J. Scheeres, S. Abe, O. Barnouin-Jha, A. F. Cheng, H. Demura, R.
581 W. Gaskell, N. Hirata, M. Ishiguro, T. Michikami, A. M. Nakamura, R. Nakamura, J.
582 Saito & S. Sasaki (2007) Regolith Migration and Sorting on Asteroid Itokawa.
583 *Science,* 316**,** 1011-1014.
584 Murchie, S. L., P. C. Thomas, A. S. Rivkin & N. L. Chabot. 2015. Phobos and Deimos. In
585 *Asteroids IV*, 451.
586 Nayak, M., F. Nimmo & B. Udrea (2016) Effects of mass transfer between Martian satellites
587 on surface geology. *Icarus,* 267**,** 220-231.
588 Phillips, R. J., R. F. Raubertas, R. E. Arvidson, I. C. Sarkar, R. R. Herrick, N. Izenberg & R.
589 E. Grimm (1992) Impact craters and Venus resurfacing history. *Journal of*
590 *Geophysical Research: Planets,* 97**,** 15923-15948.
591 Pollack, J. B., J. Veverka, M. Noland, C. Sagan, T. C. Duxbury, C. H. Acton, G. H. Born, W. K.
592 Hartmann & B. A. Smith (1973) Mariner 9 television observations of Phobos and
593 Deimos, 2. *Journal of Geophysical Research,* 78**,** 4313-4326.
594 Pollack, J. B., J. Veverka, M. Noland, C. Sagan, W. K. Hartmann, T. C. Duxbury, G. H. Born,
595 D. J. Milton & B. A. Smith (1972) Mariner 9 television observations of Phobos and
596 Deimos. *Icarus,* 17**,** 394-407.
597 Richardson, J. E., H. J. Melosh & R. Greenberg (2004) Impact-Induced Seismic Activity on
598 Asteroid 433 Eros: A Surface Modification Process. *Science,* 306**,** 1526-1529.
599 Richardson, J. E., H. J. Melosh, R. J. Greenberg & D. P. O'Brien (2005) The global effects of
600 impact-induced seismic activity on fractured asteroid surface morphology. *Icarus,*

179, 325-349.

Salamunićcar, G., S. Lončarić, P. Pina, L. Bandeira & J. Saraiva (2014) Integrated method for crater detection from topography and optical images and the new PH9224GT catalogue of Phobos impact craters. *Advances in Space Research,* 53, 1798-1809.

Schmedemann, N., G. G. Michael, B. A. Ivanov, J. B. Murray & G. Neukum (2014) The age of Phobos and its largest crater, Stickney. *Planetary and Space Science,* 102, 152-163.

Squyres, S. W., C. Howell, M. C. Liu & J. J. Lissauer (1997) Investigation of Crater "Saturation" Using Spatial Statistics. *Icarus,* 125, 67-82.

Stooke, P. (2012), Stooke Small Bodies Maps V2.0. MULTI-SA-MULTI-6-STOOKEMAPS-V2.0. NASA Planetary Data System (http://sbn.psi.edu/pds/asteroid/MULTI_SA_MULTI_6_STOOKEMAPS_V2_0/data/m2deimos/)

Thomas, P. C. (1979) Surface features of Phobos and Deimos. *Icarus,* 40, 223-243.

Thomas, P. C. (1989) The shapes of small satellites. *Icarus,* 77, 248-274.

Thomas, P. C. (1993) Gravity, Tides, and Topography on Small Satellites and Asteroids: Application to Surface Features of the Martian Satellites. *Icarus,* 105, 326-344.

Thomas, P. C. (1998) Ejecta Emplacement on the Martian Satellites. *Icarus,* 131, 78-106.

Thomas, P. C., D. Adinolfi, P. Helfenstein, D. Simonelli & J. Veverka (1996) The Surface of Deimos: Contribution of Materials and Processes to Its Unique Appearance. *Icarus,* 123, 536-556.

Thomas, P. C. & J. Veverka (1977) Phobos: Surface density of impact craters. *Icarus,* 30, 595-597.

Thomas, P. C. & J. Veverka (1980a) Crater densities on the satellites of Mars. *Icarus,* 41, 365-380.

Thomas, P. C. & J. Veverka (1980b) Downslope movement of material on Deimos. *Icarus,* 42, 234-250.

Trask, N. J. (1966) Size and Spatial Distribution of Craters Estimated From the Ranger Photographs. In Ranger VIII and IX. Part II - Experimenters' analyses and interpretations. Jet Propulsion Laboratory Technical Report No. 32-800, pp. 252-263.

Veverka, J. & T. C. Duxbury (1977) Viking observations of Phobos and Deimos: Preliminary results. *Journal of Geophysical Research,* 82, 4213-4223.

Willner, K., J. Oberst, M. Wählisch, K. Matz, H. Hoffmann, T. Roatsch, R. Jaumann, & V. Mertens (2008) New astrometric observations of Phobos with the SRC on Mars Express. *Astronomy and Astrophysics*, 488, 361-364.